



GPO PRICE \$ _____

CFSTI PRICE(S) \$ _____

Hard copy (HC) 2.00Microfiche (MF) 1.50

653 JULY 65

TECHNICAL MEMORANDUM

X-295

STATIC STABILITY AND CONTROL CHARACTERISTICS OF
TWO LARGE-DIHEDRAL RIGHT TRIANGULAR PYRAMID
LIFTING REENTRY CONFIGURATIONS AT A
MACH NUMBER OF 3.05

By Charles F. Whitcomb and Willard E. Foss, Jr.

Langley Research Center
Langley Field, Va.

Declassified by authority of NASA
Classification Change Notices No. 64

Dated 6/27/66

DECLASSIFIED- AUTHORITY
US: 1286 DROBKA TO LEBOW
MEMO DATED
7/8/66

N66 33317

FACILITY FORM 602

(ACCESSION NUMBER)

(PAGES)

(NASA CR OR TMX OR AD NUMBER)

(THRU)

(CODE)

(CATEGORY)

NATIONAL AERONAUTICS AND SPACE ADMINISTRATION
WASHINGTON

July 1960



NATIONAL AERONAUTICS AND SPACE ADMINISTRATION

TECHNICAL MEMORANDUM X-295

STATIC STABILITY AND CONTROL CHARACTERISTICS OF
TWO LARGE-DIHEDRAL RIGHT TRIANGULAR PYRAMID
LIFTING REENTRY CONFIGURATIONS AT A

MACH NUMBER OF 3.05*

By Charles F. Whitcomb and Willard E. Foss, Jr.

SUMMARY

33317

An investigation has been conducted in the Langley 9- by 12-inch blowdown tunnel at a Mach number of 3.05 on two large-dihedral right triangular pyramid models to determine the stability characteristics with and without deflection of base-mounted controls.


The investigation showed that the static longitudinal stability characteristics of the two models were generally satisfactory and the characteristics for one of the models agreed well with a similar model tested at low speeds. The model with the lesser leading-edge sweep and the higher aspect ratio had a lower maximum lift-drag ratio. The controls investigated on these models appear to be capable of trimming the models at lift coefficients and angles of attack in a region where decreased heat transfer occurs for vehicles of this shape. The roll effectiveness of the controls on one of the models decreases to adverse effectiveness at an angle of attack slightly above zero lift, and large adverse yawing-moment coefficients occur throughout the test angle-of-attack range.

Authoc

INTRODUCTION

A program is being conducted by the National Aeronautics and Space Administration to provide information on various manned, lifting reentry configurations. The present investigation was made to provide some static stability and control information at a Mach number of 3.05 on

* Title, Unclassified.





two right triangular pyramid models conceived from the heat-transfer considerations of reference 1. The lower surfaces of the models have 45° dihedral and the upper surface is flat. Leading-edge sweep of these models was 79.3° and 75.0° . Static longitudinal stability characteristics on somewhat similar models have been presented for the low speed range in reference 2 and for a Mach number of 6.2 in reference 3. The models of the present investigation incorporated a rounded lower-surface ridge line similar to that for the model in reference 3. The model for the tests of reference 2 had a sharp ridge line.

Data presented include longitudinal, lateral, and directional stability characteristics for one of the models and longitudinal characteristics only for the second model. The models were adapted with base-mounted controls tested with and without deflection. The angle of attack of the lower-surface ridge line was varied between -6° and 22° and for the more highly swept model the angle of sideslip was varied between -5° and 20° .

SYMBOLS

All coefficients presented in this paper are based on the projected plan-form area of the models. Stability data are referred to the wind-axis system for the longitudinal tests and to the body-axis system for the sideslip tests. The origin of the axis system in both cases was located to correspond to a longitudinal center-of-gravity position of 45 percent of the mean aerodynamic chord and to a vertical position on a line connecting the centroid of the base to the apex of the model.

b model span, in.

\bar{c} model mean aerodynamic chord, in.

C_L lift coefficient, $\frac{\text{Lift}}{qS}$

$(C_L)_{\text{trim}}$ lift coefficient at zero pitching moment

C_D drag coefficient, $\frac{\text{Drag}}{qS}$

C_m pitching-moment coefficient, $\frac{\text{Pitching moment}}{qS\bar{c}}$

$C_{m,0}$ pitching-moment coefficient at zero lift





C_n	yawing-moment coefficient, $\frac{\text{Yawing moment}}{qSb}$
C_l	rolling-moment coefficient, $\frac{\text{Rolling moment}}{qSb}$
C_Y	side-force coefficient, $\frac{\text{Side force}}{qS}$
L/D	lift-drag ratio
$(L/D)_{\max}$	maximum lift-drag ratio
M	Mach number
q	dynamic pressure, lb/sq in.
R	radius
S	projected plan-form area of model (not including flaps), sq in.
x_{ac}/\bar{c}	location of aerodynamic center, fraction of mean aerodynamic chord measured from leading edge
α	angle of attack of model ridge line, deg (See fig. 1.)
β	angle of sideslip (positive when nose deflected left), deg
δ_N	nominal control deflection relative to adjacent surface (positive when control deflected inward), deg
$C_{L_\alpha} = \frac{\partial C_L}{\partial \alpha}$	per degree
$C_{n_\beta} = \frac{\partial C_n}{\partial \beta}$	per degree
$C_{l_\beta} = \frac{\partial C_l}{\partial \beta}$	per degree
$C_{Y_\beta} = \frac{\partial C_Y}{\partial \beta}$	per degree





APPARATUS AND METHODS

Models

Two models were investigated. Model 1 had a leading-edge sweep of 79.3° and model 2 had a leading-edge sweep of 75.0° . Figure 1 and table I present the dimensional details. The models, which were constructed of brass, were equipped with rectangular-slab-type controls located at the trailing edge of each of the three surfaces. Dimensional details of the controls are presented in figure 1 and photographs of the models with upper-surface controls deflected are presented in figure 2.

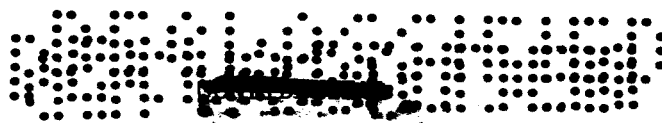
For both models, transition strips of carborundum grit were placed on the lower surfaces. The photographs of figure 2 show the location of the strips across the curved ridge line through the points of tangency of the curved apex with the model leading edge and along the lines where the curved ridge line becomes tangent to the large dihedral surfaces. The size of the grit was about 0.002 inch. Preliminary visual flow studies indicated that no strip was necessary on the flat upper surface because turbulent flow already existed.

Tests

The investigation was conducted in the Langley 9- by 12-inch blow-down tunnel at a Mach number of 3.05 at a stagnation pressure of 50 pounds per square inch absolute. The corresponding Reynolds number based on mean aerodynamic chord was 4.3×10^6 for model 1 and 3.5×10^6 for model 2. The mean aerodynamic chord was 6.6 inches for model 1 and 5.4 inches for model 2. The angle of attack was varied from -6° to 22° and for model 1 the angle of sideslip was varied from -5° to 20° . Stability information was obtained for both models with all controls set at 0° deflection. The stability characteristics with controls deflected were determined by using 20° settings of several control configurations. Excessive balance loads in the longitudinal tests of model 2 limited the negative deflection angle of the upper-surface control to -10° . For this model positive deflection of this control was also reduced to 10° for one test condition while for another test condition the deflection was 20° .

The models were mounted on a six-component internal strain-gage balance which in turn was sting mounted to the model-support system. The mechanically set angles of attack were corrected for sting and balance deflections under load and for a tunnel downflow angle of 0.5° . The data were adjusted to a condition of free-stream static pressure at the base of the model. The estimated maximum errors of the quantities presented in this paper are as follows:

[REDACTED]



M	±0.02
C _L	±0.005
C _D	±0.002
C _m	±0.001
C _n	±0.001
C _l	±0.001
C _y	±0.001
α, deg	±0.10
β, deg	±0.10

RESULTS AND DISCUSSION

Longitudinal Characteristics

The longitudinal characteristics of the two models with undeflected controls are presented in figure 3. Model 2, which has the lesser leading-edge sweep and the higher aspect ratio, has the higher lift-curve slope. The slopes listed in table II, which presents a summary of the test data, were determined near zero lift. The slope of 0.020 for model 1 is about 17 percent higher than that for the somewhat similar model with a trailing-edge extension (referred to as a 0° boattail) tested at a Mach number of 6.2 in reference 3. This difference is attributed to the decrease in lift-curve slope with increasing Mach number. Model 2, having the higher aspect ratio, has a larger frontal area and a resultant higher minimum C_D than model 1. (See fig. 3.) This increase in minimum C_D was not overcome by the lower drag due to lift of the model with the higher aspect ratio and consequently model 1 had the higher values of (L/D)_{max} - 3.4 as compared to 2.8 for model 2. (See table II.) This value for model 1 is of the order of the values obtained for the models with trailing-edge extensions of the lower and higher speed tests of references 2 and 3, respectively. The aerodynamic center of model 1 is located at about 0.57c, which is almost exactly the same location as for the model with extensions tested in reference 2 at low speeds. For the model with extensions tested in reference 3 at M = 6.2, the aerodynamic center was farther rearward at 0.63c. The location is 0.61c for model 2 of the present tests.

The longitudinal characteristics of model 1 with deflected controls are presented in figure 4 and for model 2 in figure 5. Deflections of the controls were inward (plus) or outward (minus) 20° except for the previously mentioned case of two model 2 configurations for which the inward and outward deflections of the upper-surface control were 10°. The results which are summarized in table II indicate that deflection of the pitch controls affected the aerodynamic-center location of the



models as well as the $C_{m,0}$ and $(C_L)_{trim}$. This change of aerodynamic-center location was not true of the tests of reference 2. The results presented in figures 4 and 5 include those for each model with all three flap controls deflected inward 20° . These tests were made to simulate a 20° boattail extension similar to the boattail extensions tested in references 2 and 3. For each model, the simulated boattail increased the $(L/D)_{max}$ (see figs. 4(c) and 5(c)) and moved the aerodynamic center forward toward the assumed center of gravity.

Heat-transfer considerations of this type of model presented in reference 1 refer to angles of attack where the reentry heat-transfer problem is reduced. This angle of attack for model 1 is 10.5° and for model 2 is about 15° . These angles of attack correspond very closely to the angles of attack and lift coefficients for trim of the two models with zero flap deflection. (See figs. 4 and 5.) Reference 1 also indicates that higher angles of attack than those indicated previously would result in a further alleviation of the heat-transfer problem. The controls as investigated are capable of trimming each of the models for angles of attack up to 23° . The controls, therefore, appear to be capable of trimming the models at lift coefficients and angles of attack in a region where reference 1 indicates decreased heat transfer.

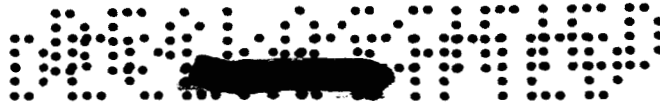
Figure 6 presents the variation of incremental rolling- and yawing-moment coefficients with angle of attack that results from deflection for roll of the lower-surface control flaps of model 1. The favorable control effectiveness decreases to an adverse effectiveness at an angle of attack of 12° or an angle a few degrees above zero lift. The deflected controls produced large adverse yawing-moment coefficients throughout the test angle-of-attack range.

Variable Sideslip Characteristics

The variation of C_n , C_l , and C_y with β for model 1 at an angle of attack of about 7.7° is presented in figure 7. The figure includes results for the model with undeflected controls and the model with lower-surface controls deflected to determine their directional effectiveness. The stability derivatives $C_{n\beta}$, $C_{l\beta}$, and $C_{y\beta}$ are listed in table II.

These slopes were obtained near an angle of sideslip of 0° . For the particular test angle of attack, the derivatives for the model with undeflected controls agree very well with the low-speed results of reference 2. The model with undeflected controls is directionally stable, and the directional stability increases with deflection of the lower-surface controls. The model has comparatively large effective dihedral on which the controls have little effect.





CONCLUSIONS

The investigation of two similar lifting reentry configurations at a Mach number of 3.05 with and without deflected controls indicates the following conclusions:

1. The static longitudinal stability characteristics of the two models were generally satisfactory and the characteristics for one of the models agreed well with a similar model tested at low speeds.
2. The model with the lesser leading-edge sweep and the higher aspect ratio had a lower maximum lift-drag ratio.
3. The controls investigated on these models appear to be capable of trimming the models at lift coefficients and angles of attack in a region where decreased heat transfer occurs for vehicles of this shape.
4. The roll effectiveness of the controls on one of the models decreases to adverse effectiveness at an angle of attack slightly above zero lift, and large adverse yawing-moment coefficients occur throughout the test angle-of-attack range.

Langley Research Center,
National Aeronautics and Space Administration,
Langley Field, Va., March 17, 1960.

REFERENCES

1. Cooper, Morton, and Stainback, P. Calvin: Influence of Large Positive Dihedral on Heat Transfer to Leading Edges of Highly Swept Wings at Very High Mach Numbers. NASA MEMO 3-7-59L, 1959.
2. Paulson, John W.: Low-Speed Static Stability and Control Characteristics of a Model of a Right Triangular Pyramid Reentry Configuration. NASA MEMO 4-11-59L, 1959.
3. Mayo, Edward E.: Static Longitudinal Stability Characteristics of a Blunted Glider Reentry Configuration Having 79.5° Sweepback and 45° Dihedral at a Mach Number of 6.2 and Angles of Attack Up to 20° . NASA TM X-222, 1959.






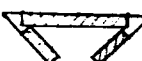


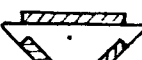
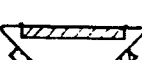
~~CONFIDENTIAL~~

TABLE I.-- DIMENSIONAL CHARACTERISTICS OF MODEL

	Model 1	Model 2
Airfoil section	Wedge	Wedge
Area (not including flap area), sq in.	20.4	21.3
Span, in.	4.02	4.91
Aspect ratio	0.79	1.13
Root chord (length), in.	8.50	7.11
Tip chord, in.	0	0
Mean aerodynamic chord, in.	6.60	5.43
Sweepback of leading edge, deg	79.3	75.0
Dihedral, deg	45	45
Control-surface chord, in.	0.945	1.00
Ridge-line radius, in.	0.63	0.75


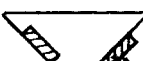
TABLE II.- SUMMARY OF TEST DATA

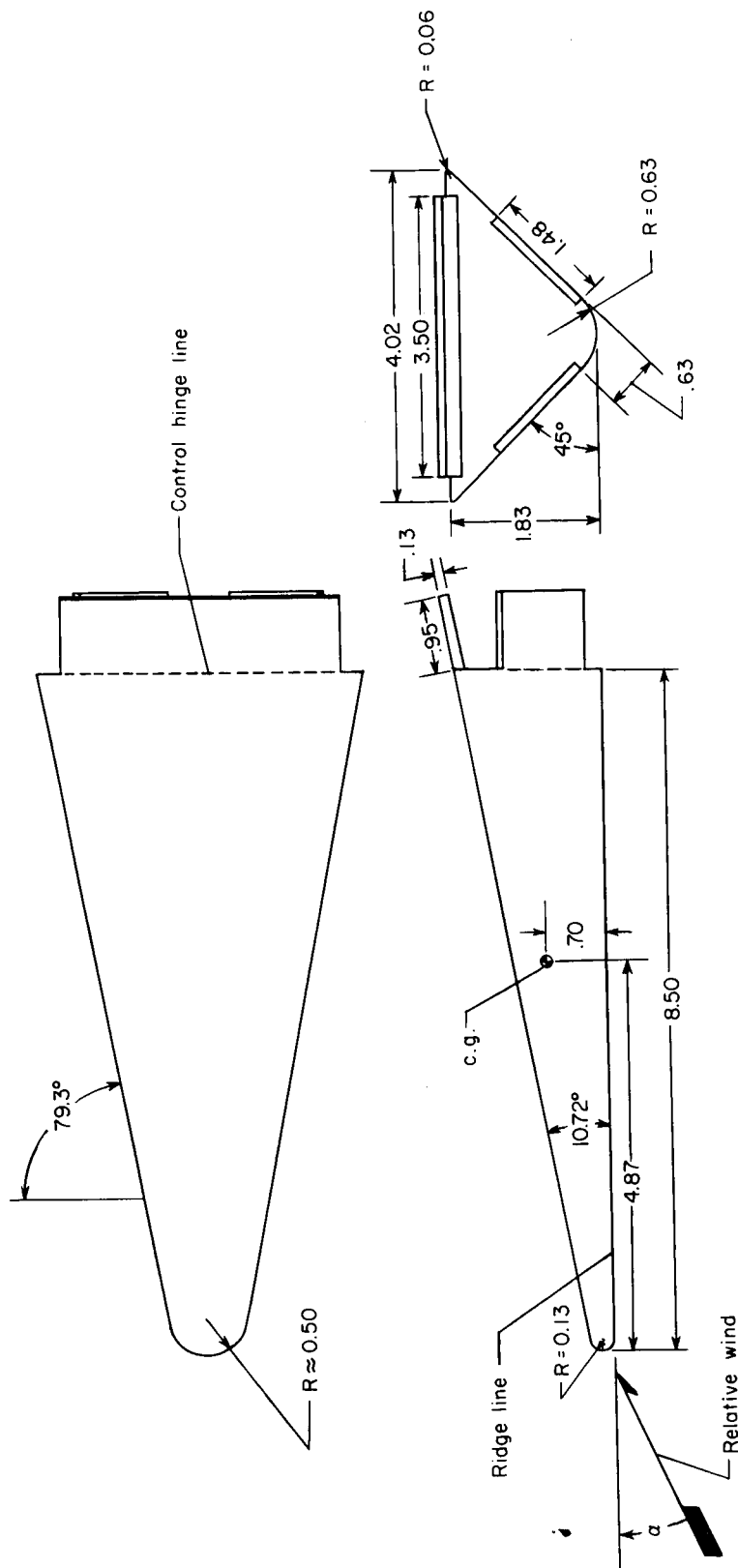
(a) Longitudinal tests

Model	Configuration ($\delta_N = 20^\circ$ except where noted)	$C_{L\alpha}$	$(L/D)_{\max}$	C_L at $(L/D)_{\max}$	$\frac{\partial C_m}{\partial C_L}$	$\frac{x_{ac}}{\bar{c}}$	$C_{m,0}$	$(C_L)_{\text{trim}}$
1		0.020	3.4	0.16	-0.117	0.567	0.008	0.07
2		.025	2.8	.21	-.156	.606	.014	.09
1		.019	3.6	.14	-.077	.527	.001	.01
2		.023	3.0	.19	-.097	.547	.003	.03
1					-.170	.620	.047	.28
1					-.112	.562	-.025	-.23
2	 $\delta_N = -10^\circ$				-.170	.620	.046	.27
2	 $\delta_N = 10^\circ$				-.156	.606	-.030	-.19

(b) Sideslip tests

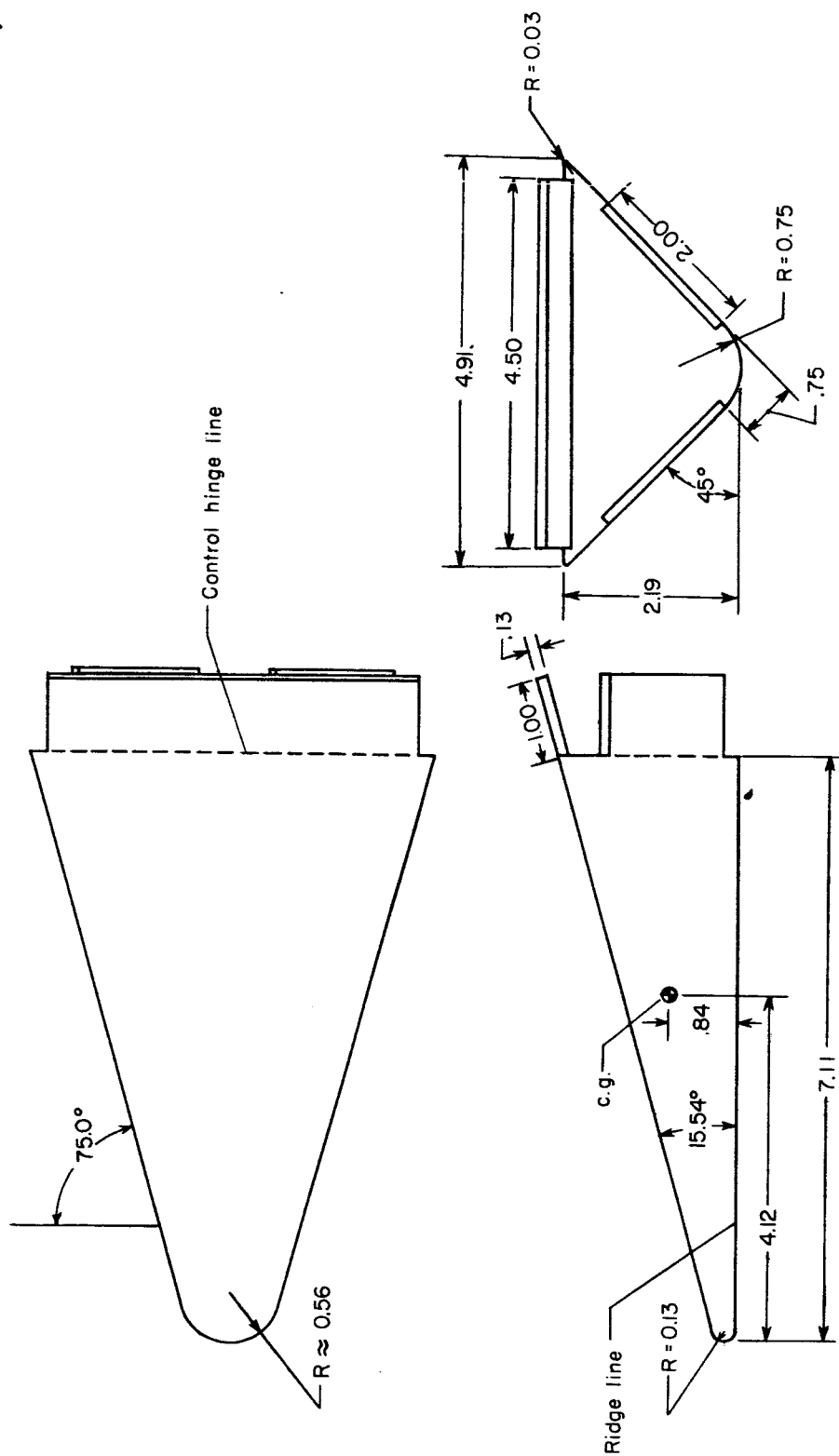
$$[\alpha \approx 7.7^\circ]$$

Model	Configuration ($\delta_N = 20^\circ$)	$C_{n\beta}$	$C_{l\beta}$	$C_{Y\beta}$
1		0.0015	-0.0015	-0.0063
1		.0022	-.0016	-.0064



(a) Model 1.

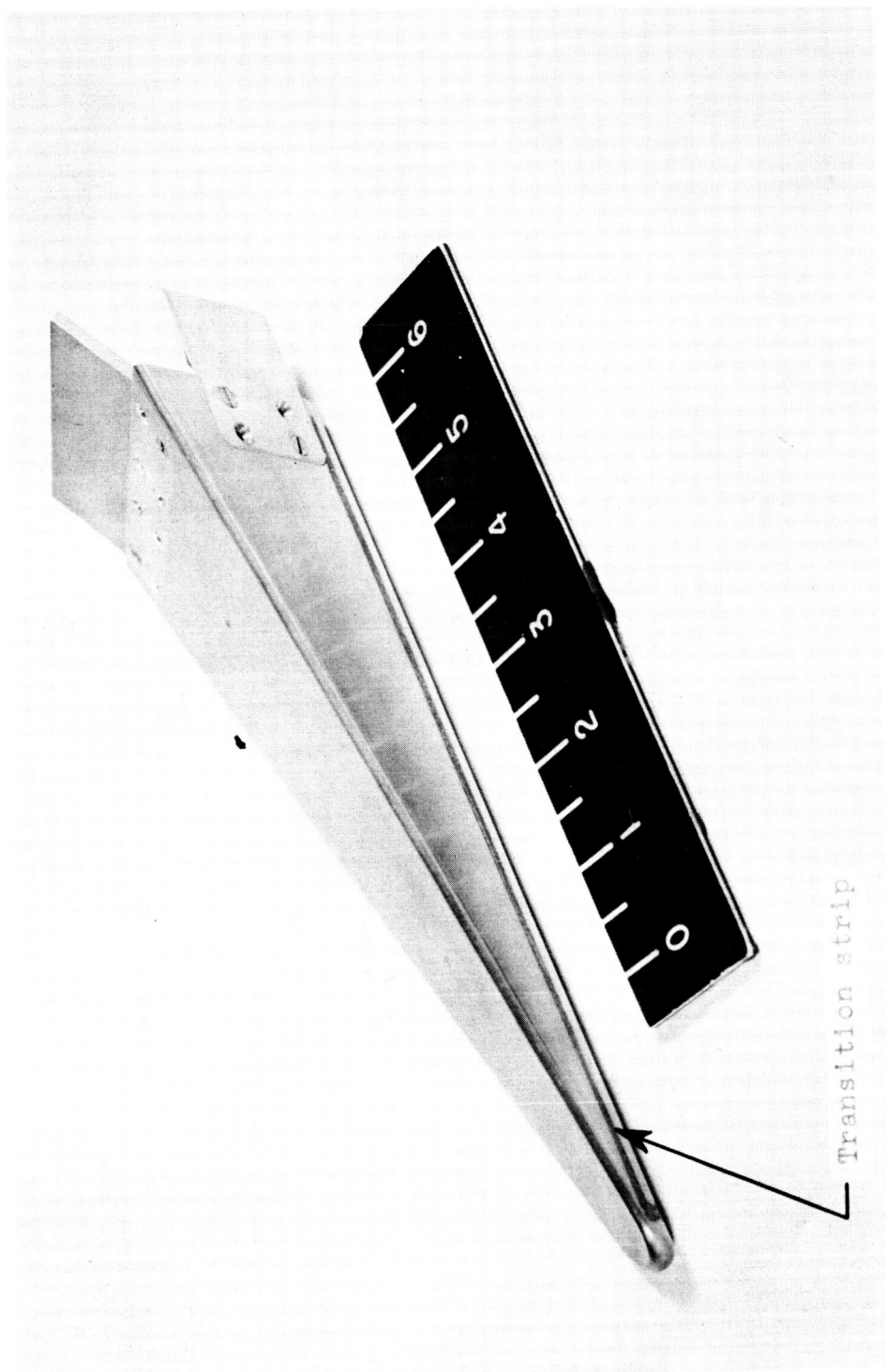
Figure 1.- Sketch of models. $\delta_N = 0^\circ$. All dimensions are in inches except where otherwise noted.



(b) Model 2.

Figure 1.- Concluded.

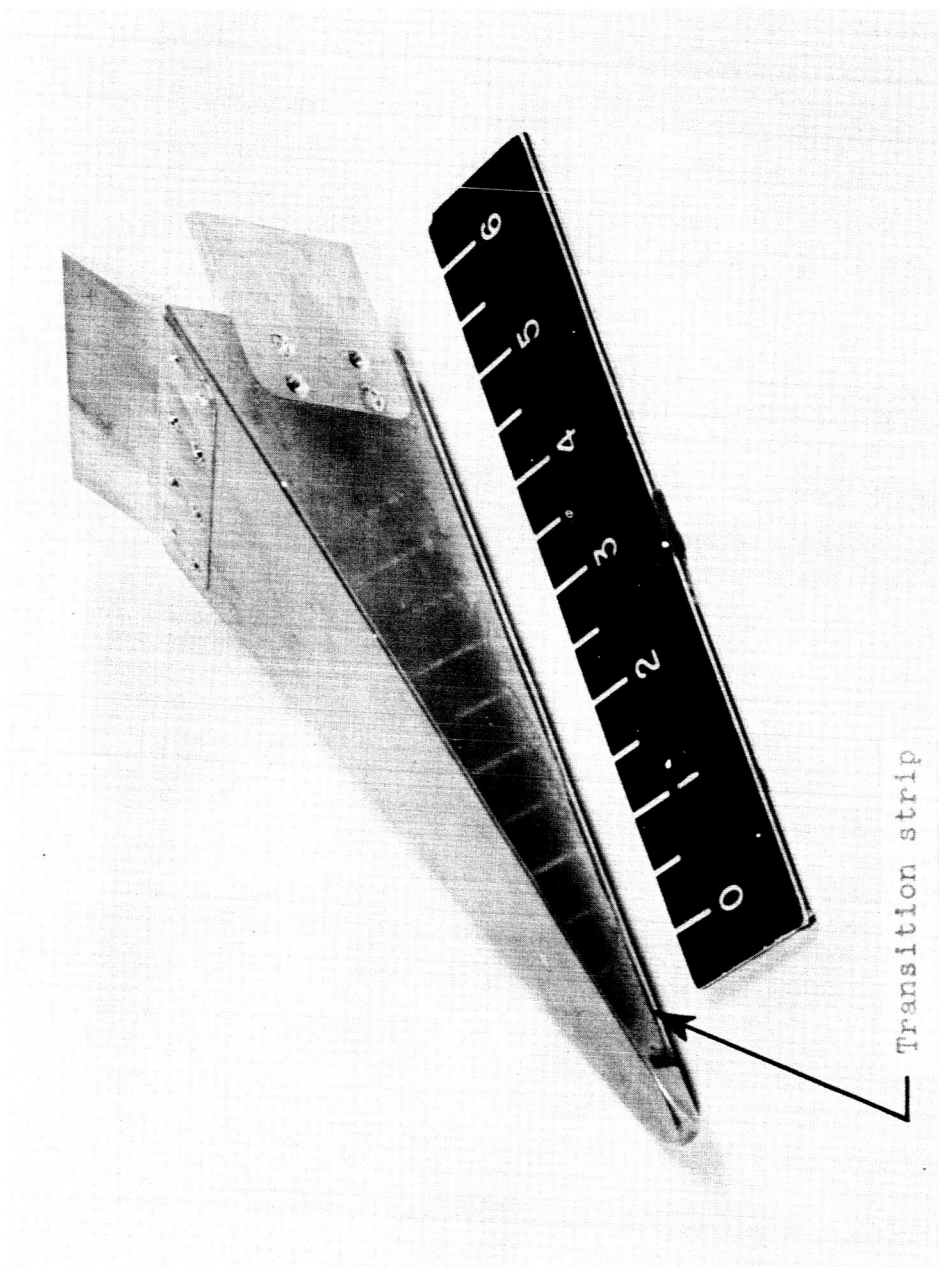
CONFIDENTIAL



(a) Model 1.

L-59-5249.1

Figure 2.- Photographs of models with upper-surface flap deflected upward 20°.



(b) Model 2.

L-59-5253.1

Figure 2.- Concluded.

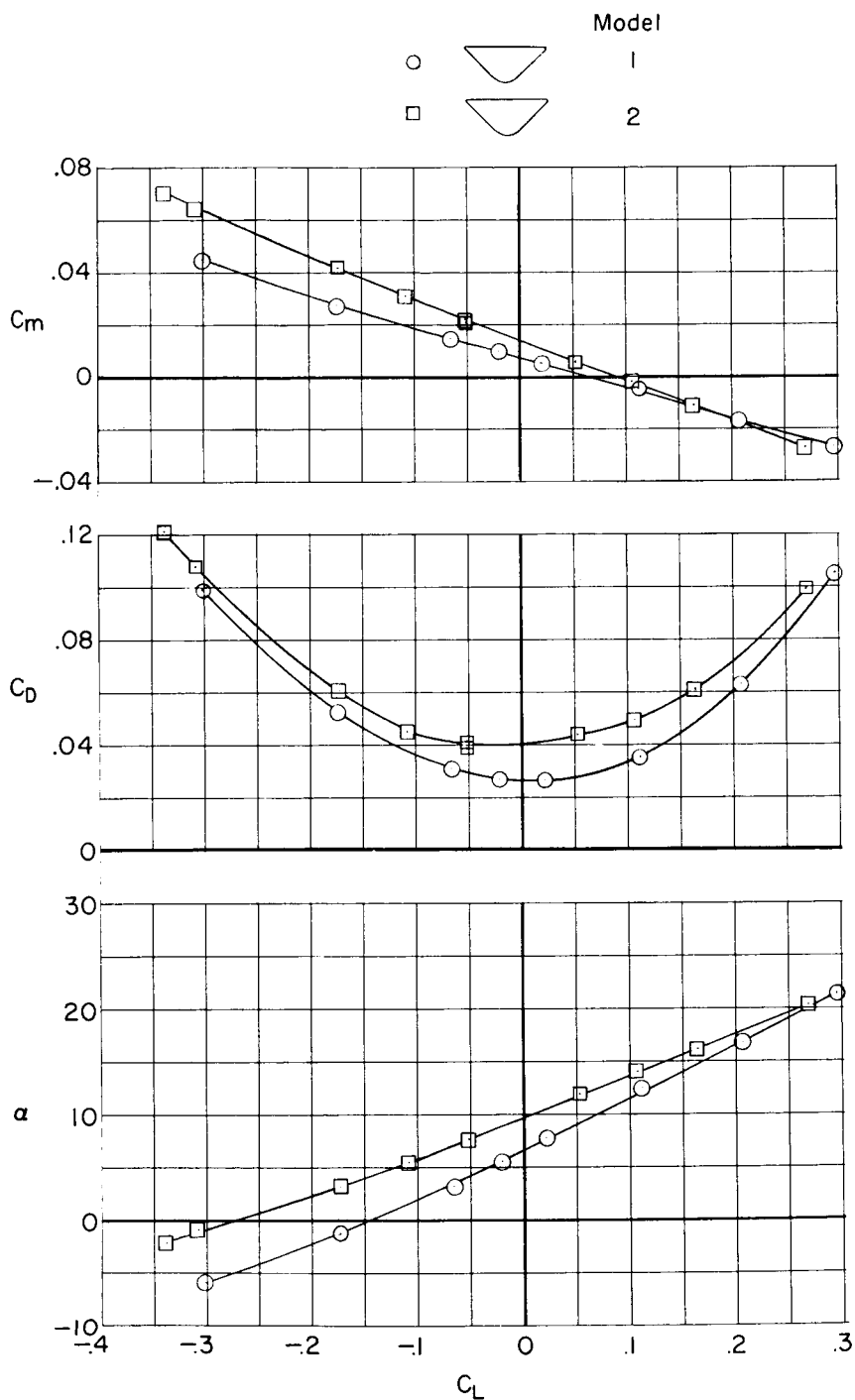
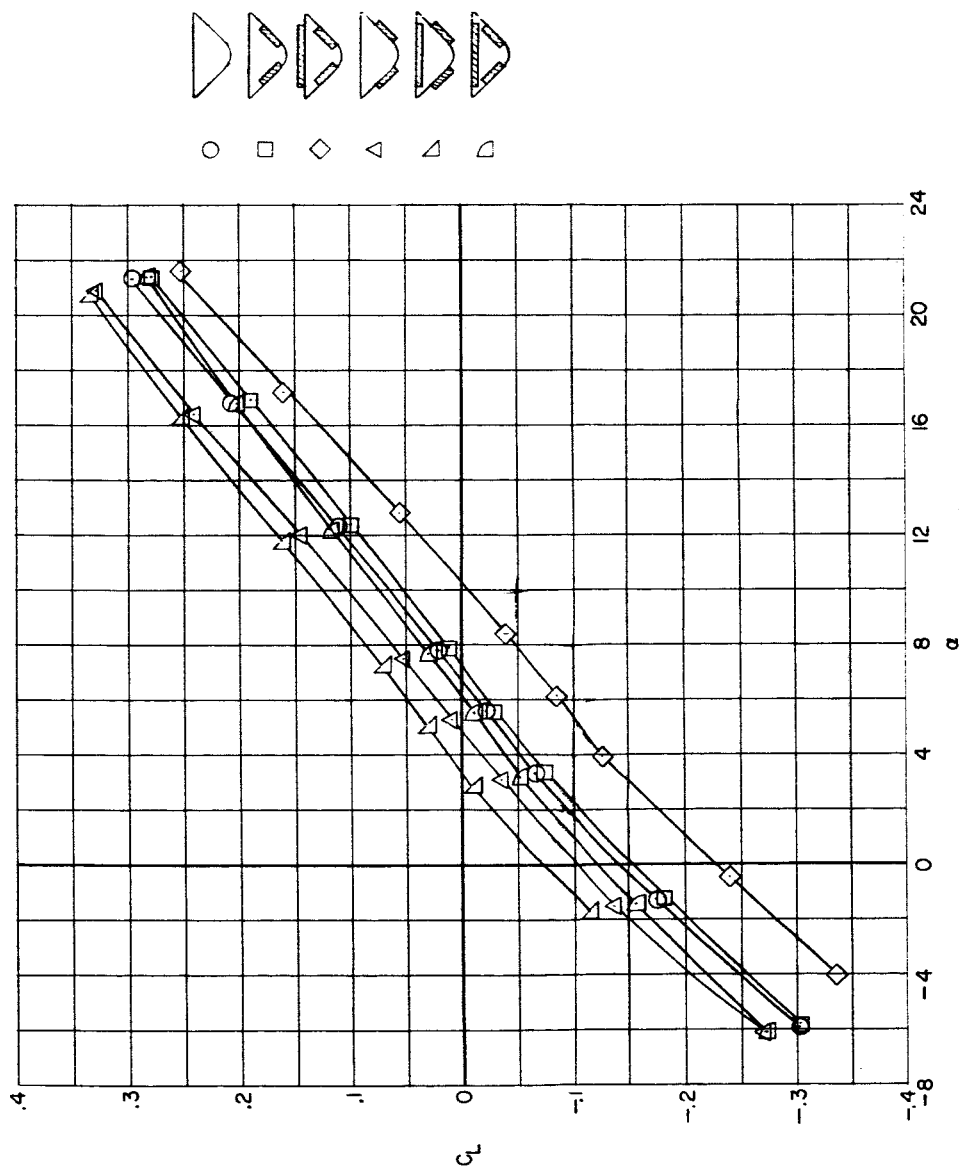
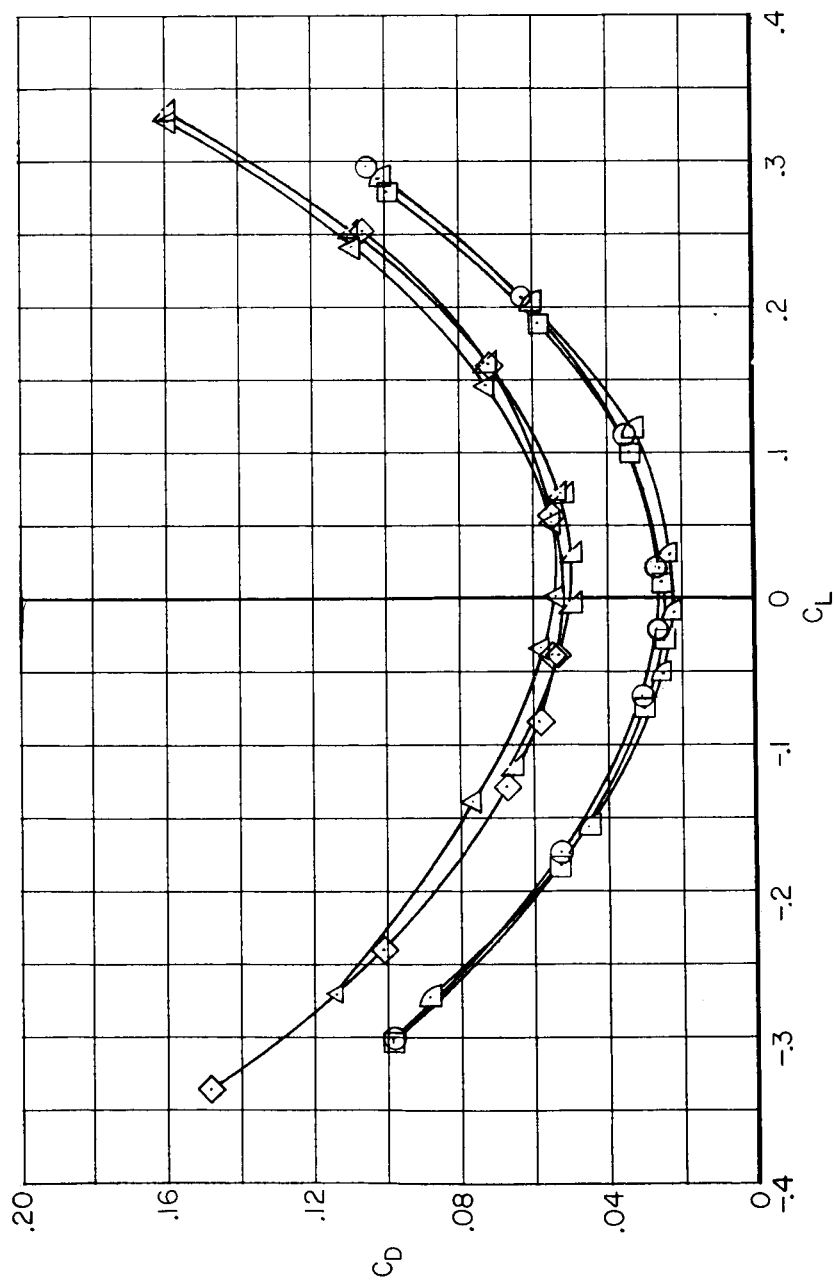


Figure 3.- Longitudinal characteristics of models with flaps at 0° deflection. $\beta = 0^\circ$.



(a) Variation of C_L with α .

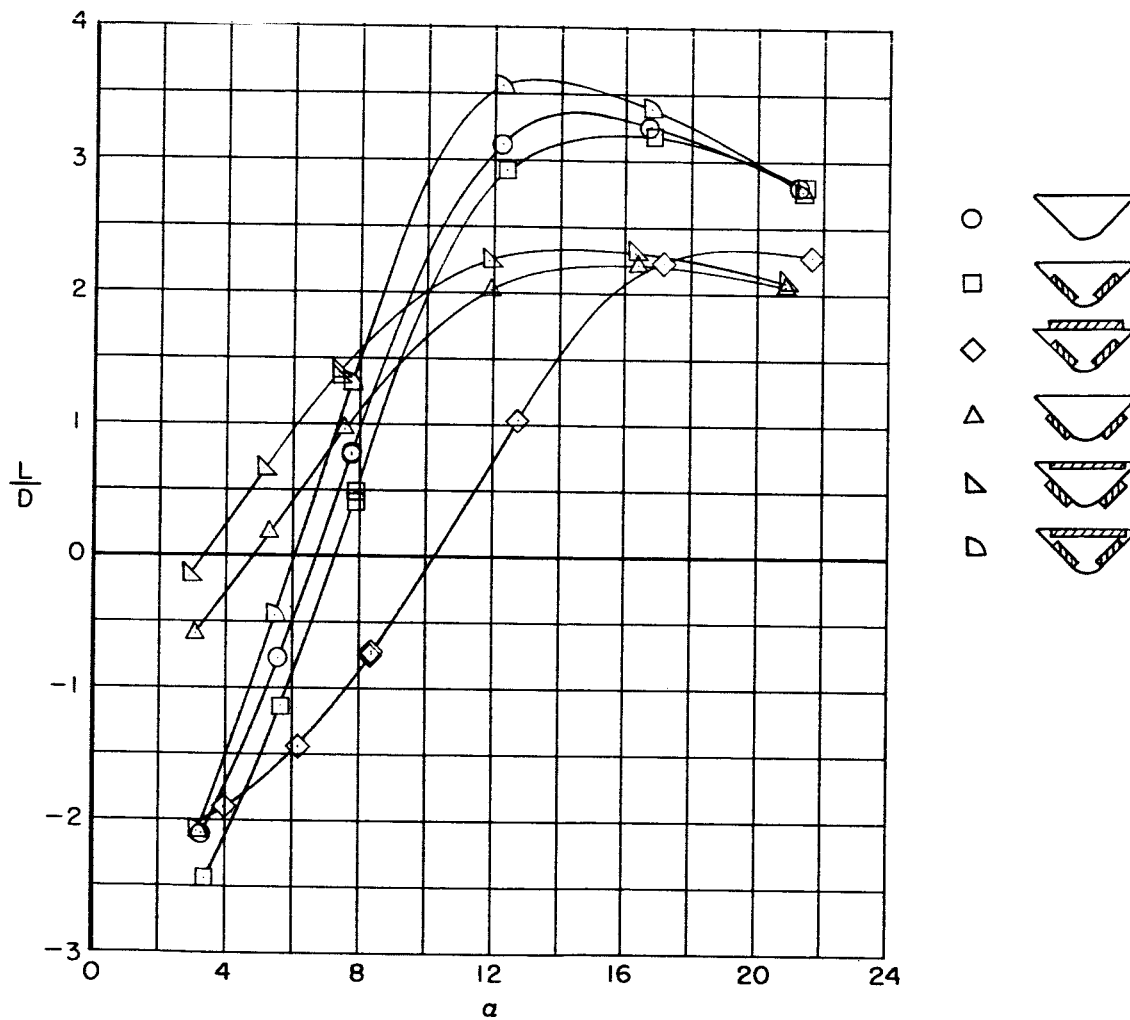
Figure 4.- Longitudinal characteristics of model 1, showing the effects of flap deflections for pitch control and simulated boattail. $\delta_N = \pm 20^\circ$; $\beta = 0^\circ$.



(b) Variation of C_D with C_L .

Figure 4.- Continued.

SECRET

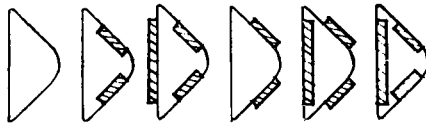


(c) Variation of L/D with α .

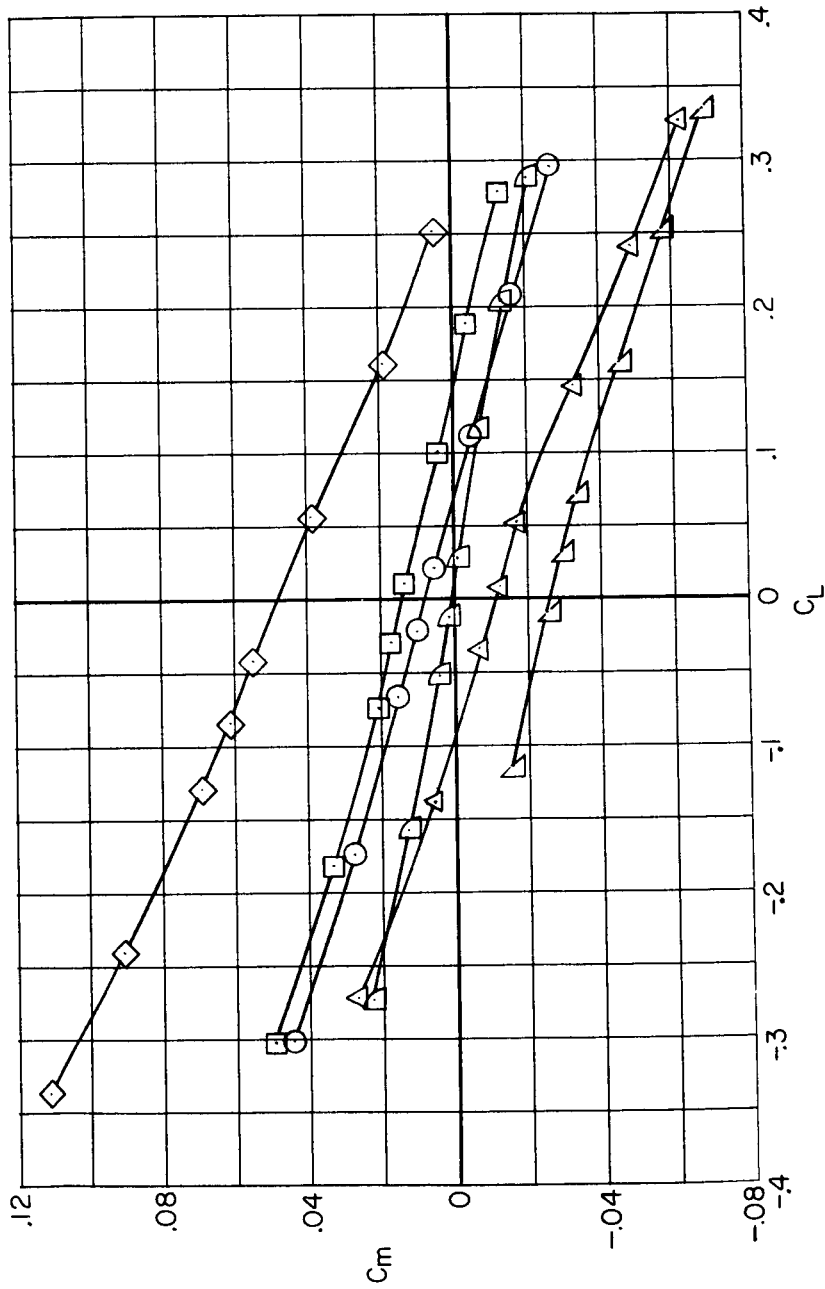
Figure 4.- Continued.

SECRET

03712030



○ □ ◇ ▲ ▴ ▽



(d) Variation of C_m with C_L .

Figure 4.- Concluded.

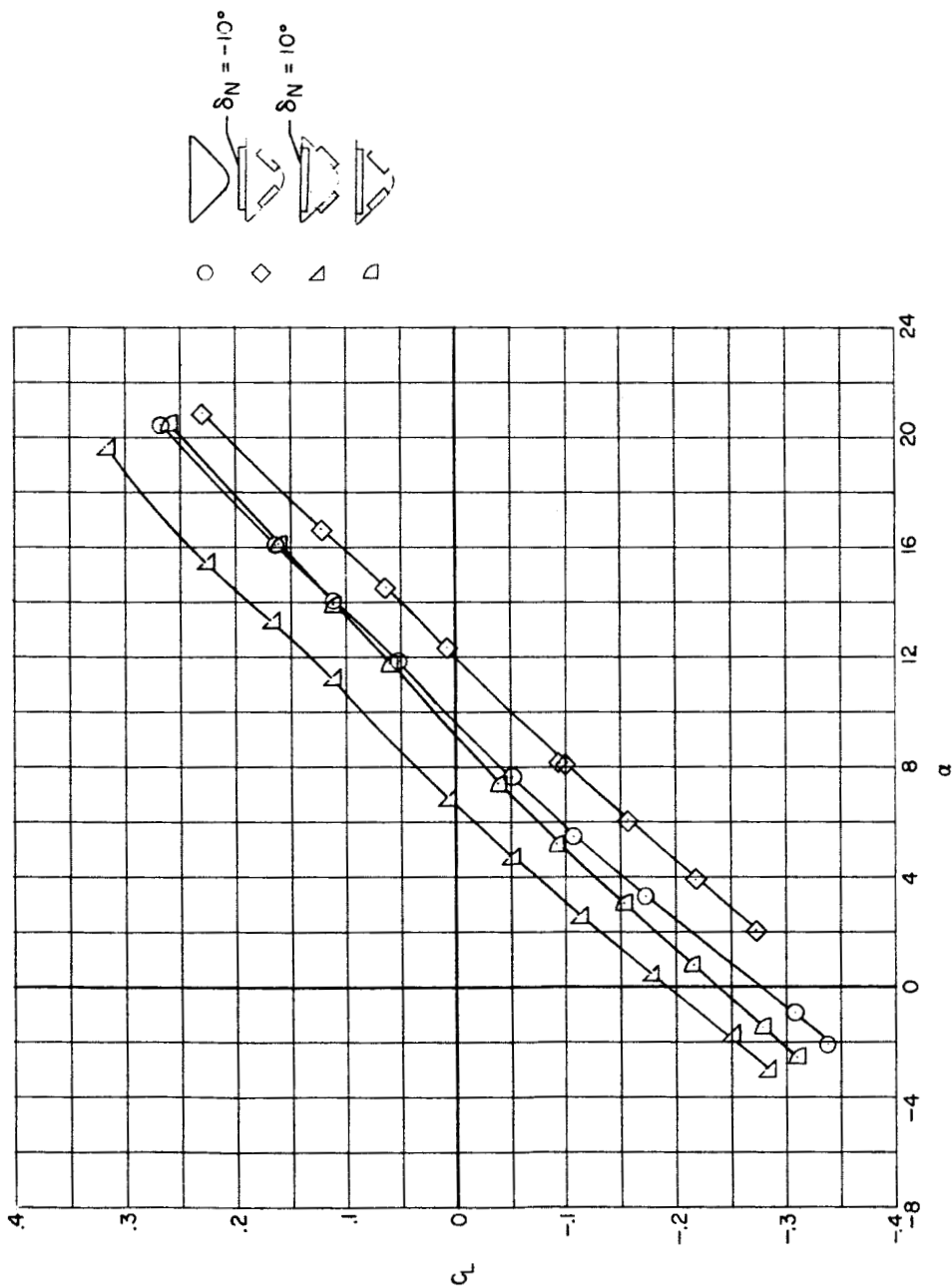
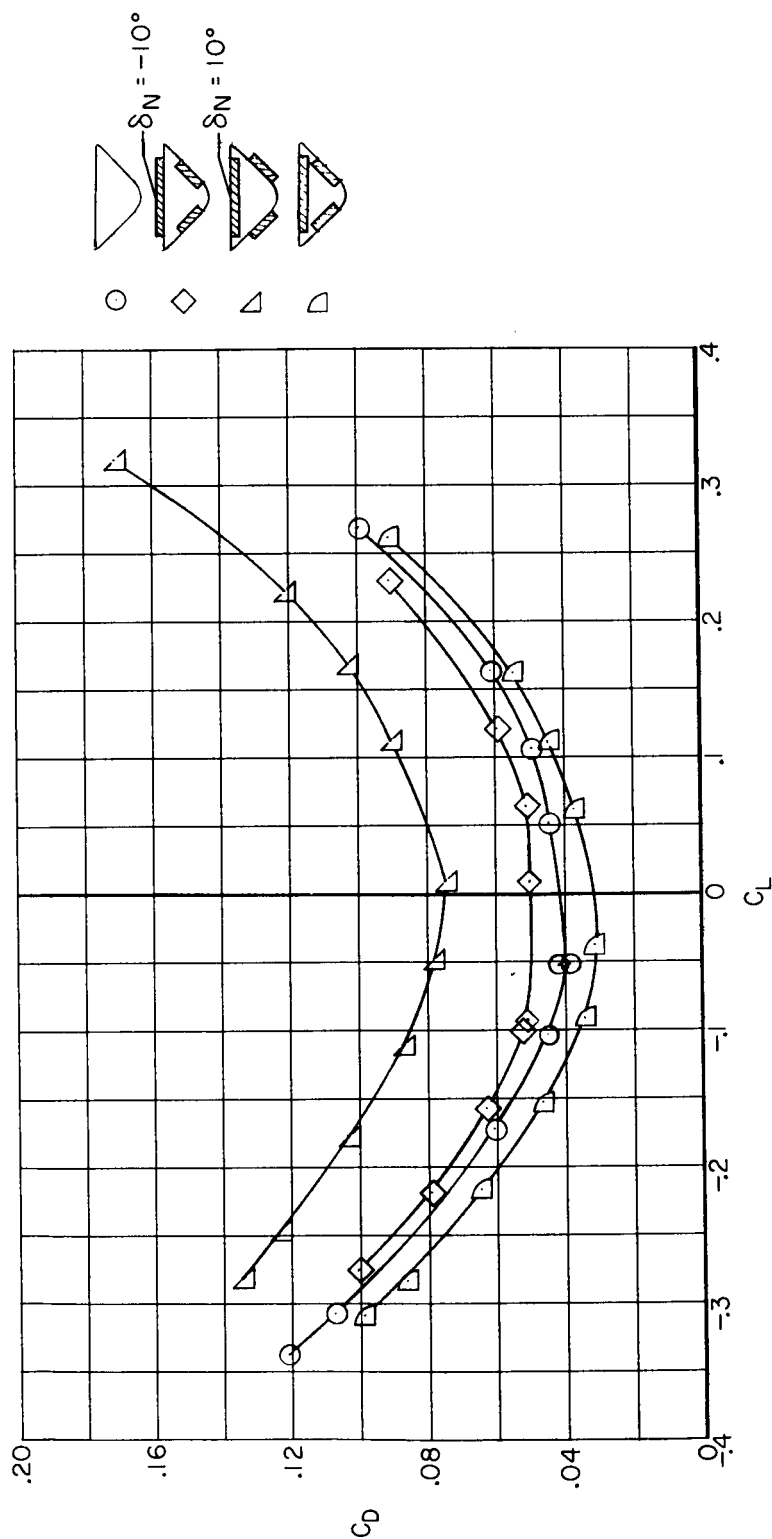
(a) Variation of C_L with α .

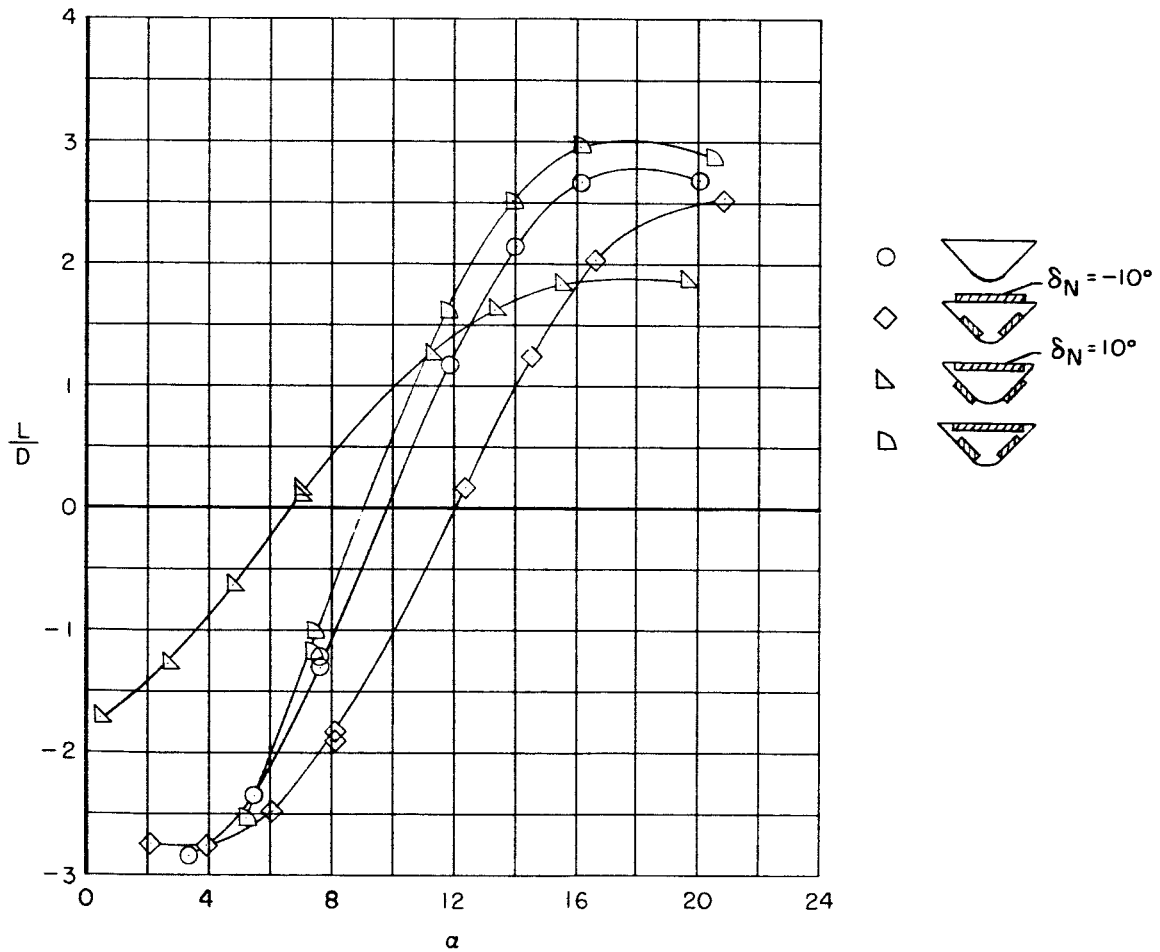
Figure 5.- Longitudinal characteristics of model 2, showing the effects of flap deflections for pitch control and simulated boattail. $\delta_N = \pm 20^\circ$ except where noted; $\beta = 0^\circ$.

037103030



(b) Variation of C_D with C_L .

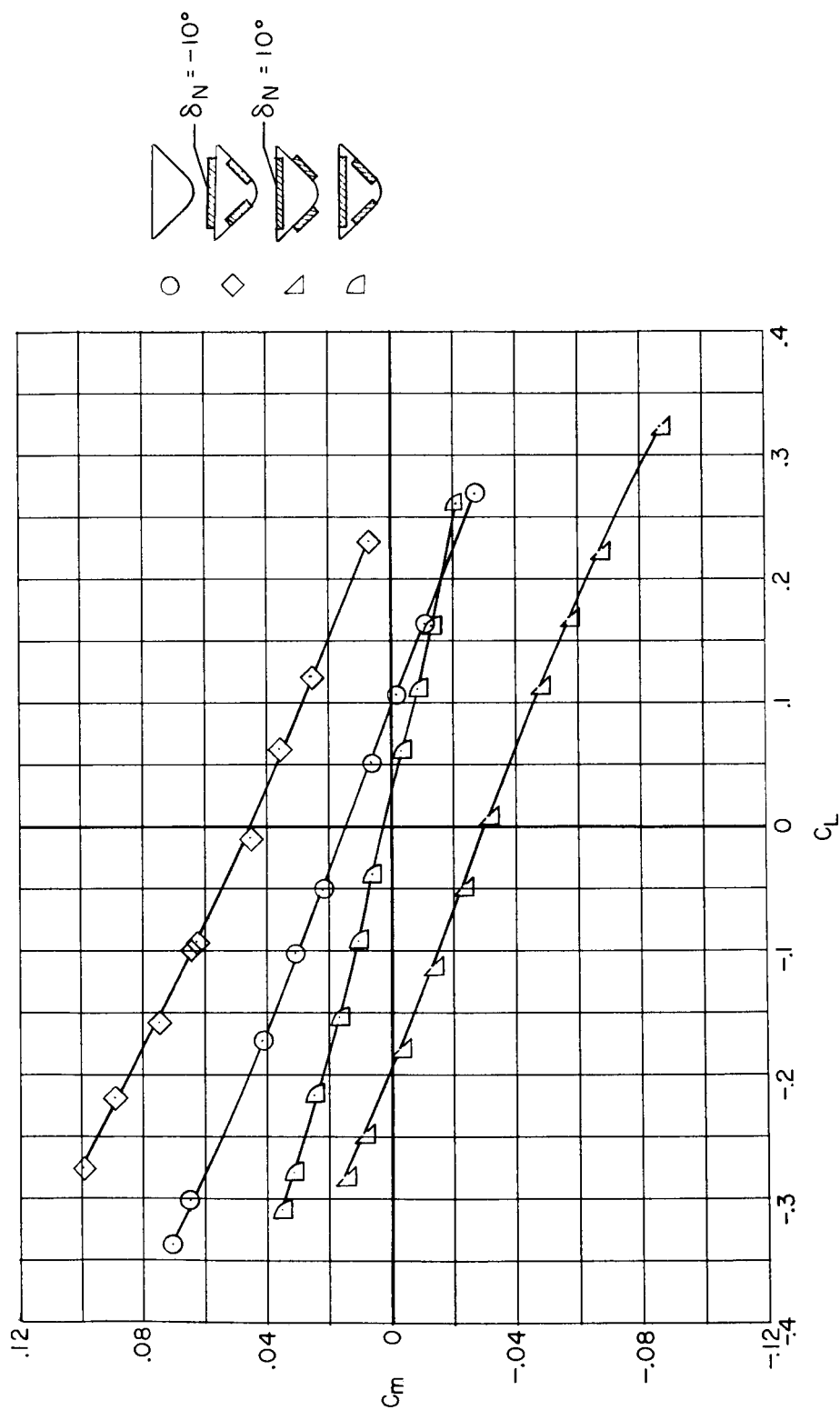
Figure 5.- Continued.



(c) Variation of L/D with α .

Figure 5.- Continued.

0371 [REDACTED] 34



(d) Variation of C_m with C_L .

Figure 5.- Concluded.

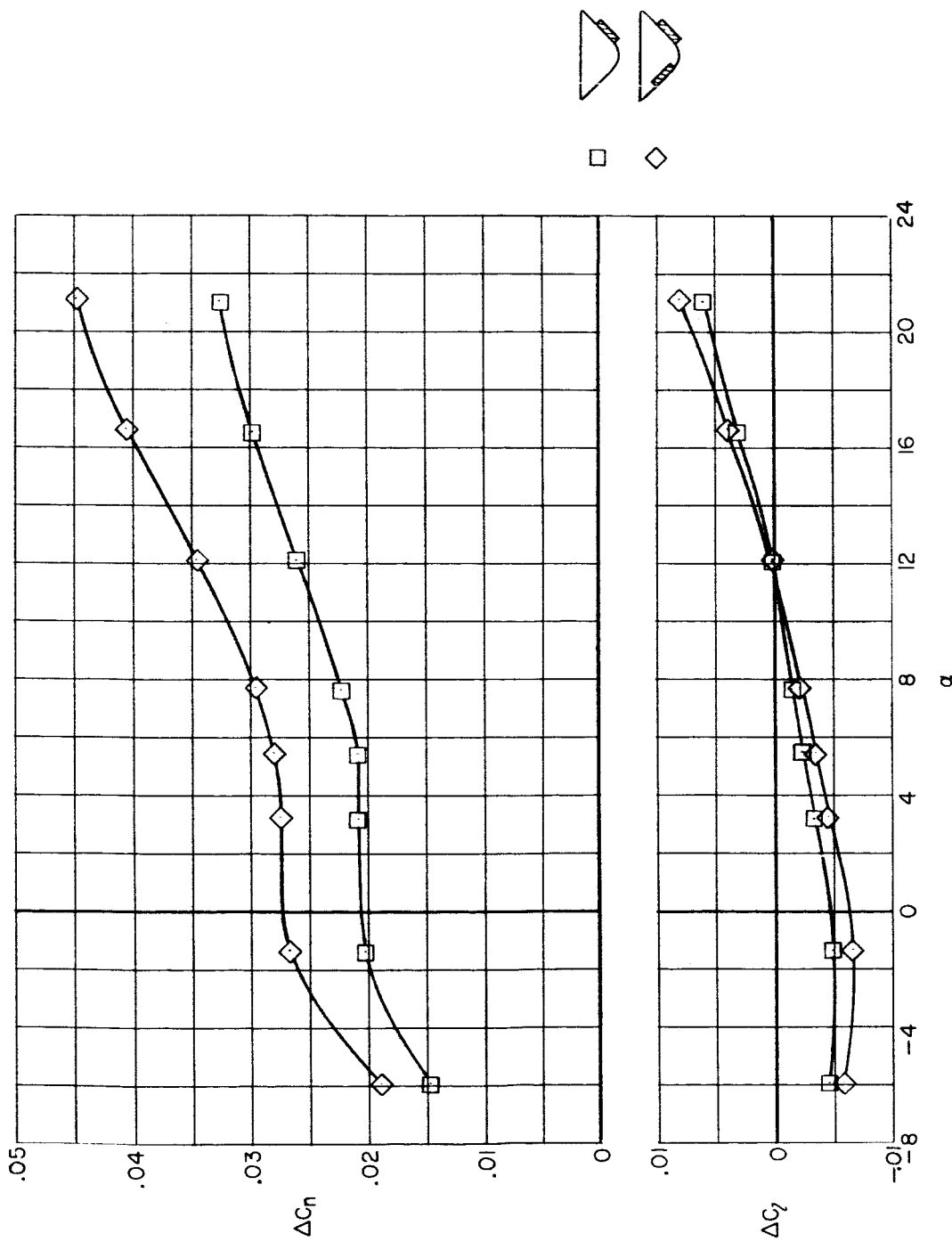


Figure 6.- Variation of incremental rolling- and yawing-moment coefficients with angle of attack for model 1 with lower-surface flaps deflected as roll controls. $\delta_N = +20^\circ$; $\beta = 0^\circ$.

[REDACTED]

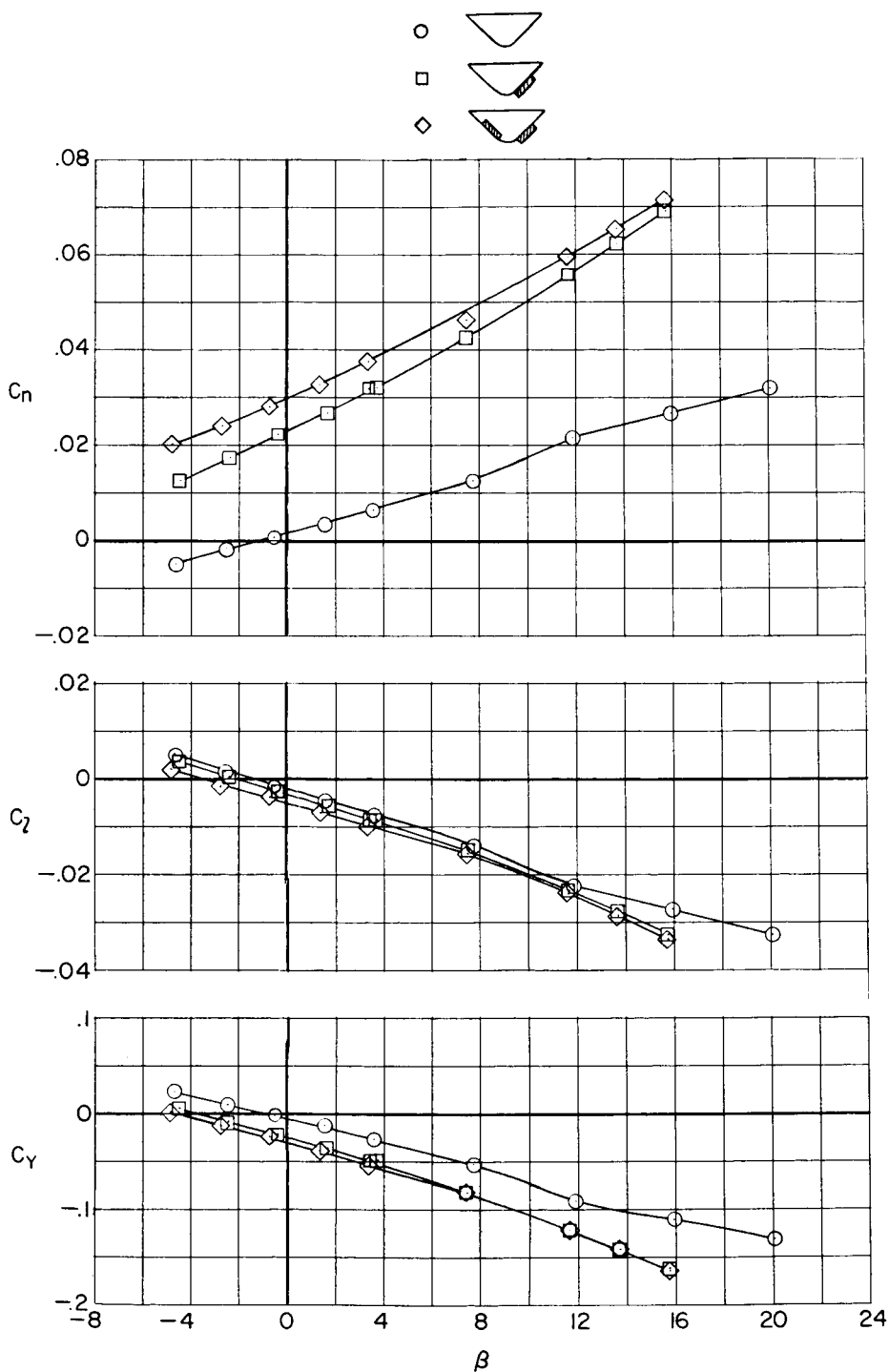


Figure 7.- Variation of C_n , C_l , and C_y with β for model 1 with lower-surface flaps deflected. $\delta_N = \pm 20^\circ$; $\alpha \approx 7.7^\circ$.